Crystal Structure of an Unusual Polytype: 7H-$Ba_7Nb_4MoO_{20}$

E. García-González, M. Parras, and J. M. González-Calbet*

Departamento de Química Inorgánica, Facultad de Ciencias Químicas, Universidad Complutense, 28040-Madrid, Spain

Received October 13, 1998. Revised Manuscript Received December 4, 1998

A new cation deficient hexagonal perovskite with the unusual polytype 7H (hhchhcc) has been obtained in the Ba−Mo−Nb−O system for the $Ba_7Nb_4MoO_{20}$ composition. It crystallizes in the $P\bar{3}m1$ space group (No. 164) with hexagonal lattice parameters $a = 5.8644(2)$ Å and $c = 16.5272(4)$ Å. The crystal structure has been studied by means of X-ray powder diffraction, electron diffraction, high-resolution electron microscopy, and neutron powder diffraction. The unit cell of $Ba_7Nb_4MoO_{20}$ can be seen as an ordered intergrowth along the *c*-axis of the structural units corresponding to the 12R and the palmierite polytypes. Both types of blocks are isolated through the cationic vacancies, giving rise to a layered structure. The existence of two cationic empty sites per unit cell is probably the reason for the 7H polytype containing two hh pairs being adopted.

Introduction

The structural polytypes adopted by cation-deficient perovskite oxides are the same as those known for the stoichiometric AMO_3 hexagonal perovskite compounds. The change in composition from ABO_3 is brought about by layers of empty octahedra in the center of the hexagonal slabs. In this sense, the structure adopted by hexagonal perovskite-like oxides with the general formula $A_nB_{n-\delta}O_{3n-x}$ ($\delta \geq 1$, $x \geq 0$) is related to the number of cationic vacancies in such a way that a hh pair is required to define the empty site. Therefore, one n term differs from the $(n + 1)$ compound in one c layer, for a given δ value.

Besides the A:B cationic ratio, the nature and the formal charge of the elements occupying the B framework determine the structural type adopted in these cationic deficient perovskites.

In the Ba−Mo−Nb−O system new compounds have been obtained for the different Nb:Mo ratios explored. The results obtained show the complex crystal chemistry of these phases to be governed by many confluent facts. Besides the above-mentioned factors, the relative stability of the different polyhedral arrangements of the Nb−Mo framework makes possible the localization of the oxygen vacancies. Thus, for an A:B::3:2 ratio, the structural type adopted ranges from the $Cs_3Tl_2O_9$-type in $Ba_3Mo_2O_9$[1] to a structure derived from the 9R polytype in $Ba_3MoNbO_{8.5}$,[1] where the flexibility of the $(hhc)_3$ stacking sequence allows the formation of a modulated structure by introducing mixed $BaO_{2.6}$ cubic layers in the 9R polytype. A 9H structure of sequence (chcchhcch) is obtained in $Ba_3Nb_2O_8$.[2] Higher A:B ratios would allow us to vary the Nb:Mo fraction in a bigger range, thus possibly leading to a better understanding of the crystal chemistry involved in this system. In this sense, the A:B::7:6 and 7:5 ratios were extensively explored, the Nb:Mo::4:1 composition, for the 7:5 ratio, being the one giving a single phase.

In the present paper we describe the results in the structural investigations of the new hexagonal perovskite-like oxide $Ba_7Nb_4MoO_{20}$. The crystal structure has been determined on the basis of the X-ray diffraction, electron diffraction, high-resolution electron microscopy, and neutron diffraction studies performed.

Experimental Section

$Ba_7Nb_4MoO_{20}$ was prepared by the solid-state reaction of $BaCO_3$ (Aldrich, 99.98%), MoO_3 (Aldrich, 99.5%), and Nb_2O_5 (Aldrich, 99.5%). Stoichiometric amounts of initial reagents were ground and the mixture was pressed into a pellet. This pellet was heated at 1300 °C for 72 h. The pale cream homogeneous product was cooled in air to room temperature in the platinum crucibles used for the synthesis.

The oxygen content was determined by thermogravimetric analysis developed on the basis of a CAHN D-200 electrobalance. The sample was reduced under a N_2 atmosphere at 900 °C. The total amount of barium, niobium, and molybdenum was determined by inductive coupling plasma (ICP) as well as by EDS X-ray microanalysis carried on a PHILIPS CM20 FEG Super Twin electron microscope.

Powder X-ray diffraction was performed on a PHILIPS X'PERT diffractometer equipped with a bent copper monochromator and using CuKα radiation.

Neutron diffraction data were collected at the Laboratoire Leon Brillouin (Saclay, France) using 2.3433 Å neutrons obtained by reflection from a Ge(004) monochromator. The diffraction profile was recorded in steps of 0.1° 2θ for the range $3° \leq 2\theta \leq 170°$, at 300 K. The peak shape was described by a pseudo-Voigt function and the background level was defined by a polynomial function. The scale factor, the counter zero point, the peak asymmetry, and the unit cell parameters were refined in addition to the atomic parameters. All the calcula-

(1) García-González, E.; Parras, M.; González-Calbet, J. M. *Chem. Mater.* **1998**, *10*, 1576.
(2) García-González, E.; Parras, M.; González-Calbet, J. M. To be published.

10.1021/cm981011i CCC: $18.00
Published on Web 01/28/1999

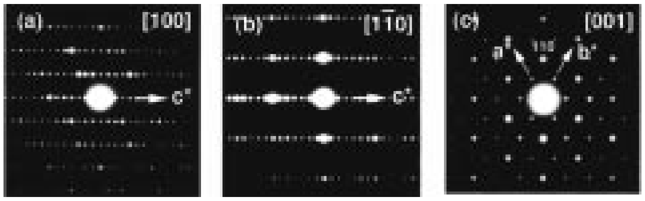

Figure 1. SAED patterns of $Ba_7Nb_4Mo\ O_{20}$ along (a) [100], (b) [1$\bar{1}$0], and [001] zone axes.

tions were performed using the program FULLPROF.[3]

Selected area electron diffraction (SAED) was carried out on a JEOL 2000FX electron microscope. High-resolution electron microscopy (HREM) was performed on both JEOL 4000EX and PHILIPS CM20 FEG Super Twin electron microscopes. In support of the interpretation of the high-resolution observations, images were simulated using the "Mac Tempas" software package. The atomic coordinates and occupancies determined by neutron diffraction were used as input data. Samples for transmission electron microscopy investigations were prepared by crushing the powder under *n*-butanol and dispersing the grains on copper grids covered with a holey carbon film.

Results and Discussion

The powder X-ray diffraction pattern revealed a single-phase sample for the nominal composition $Ba_7Nb_4MoO_{20}$. The whole pattern could be indexed on the basis of a hexagonal lattice of cell parameters $a = 5.86$ Å and $c = 16.53$ Å.

Taking into account the average value of the distance between BaO_3 layers to be 2.2−2.3 Å, the cell dimensions are consistent with a seven-layer stacking of close-packed BaO_3 layers. For the 7H type, there are a total of three possible stacking sequences, (chcccch), (hhchhcc), and (cchhhhc) [(5)(2), (3)1(2)1, and (4)1(1)1 in the Zhdanov notation[4]]. All of them correspond to the $P\bar{3}m1$ space group, which is consistent with the absence of diffraction conditions.

In terms of coordination polyhedra, the first sequence contains blocks of two pairs of face sharing octahedra linked directly by sharing corners and separated one from the next through three corners sharing octahedra. The second one is constituted by two triplets of face sharing octahedra linked directly through the corners, every two of these triplets being separated by one corner sharing octahedra. The last stacking sequence is formed by strips of five face sharing octahedra linked by two corner sharing octahedra.

Although the three 7H polytypes described are in agreement with the unit cell derived from the X-ray diffraction data, the first one seems to be less probable if we consider, as it has been already mentioned in the Introduction, that the hexagonal cation-deficient perovskite-like oxides stabilize structures which contain at least two consecutive h layers.

To elucidate the layer sequence of the structure, an electron microscopy study was performed. Figure 1 a−c corresponds to the [100], [1$\bar{1}$0], and [001] zone axes. All the diffraction maxima can be indexed on the previously defined unit cell. The three most relevant zone axes of the hexagonal structure are then in agreement with the above symmetry as well as the absence of systematic extinctions.

The most informative high-resolution images are those taken along the close-packed directions of the layers. HREM images of $Ba_7Nb_4MoO_{20}$ have been obtained along the [100] and [1$\bar{1}$0] zones. They are shown in Figures 2a and 3a, respectively.

All the crystals studied appeared to be well-ordered. In the [100] zone, the structure is viewed along the Ba−O−Ba rows and the image directly reveals the stacking sequence. The bright dots of Figure 2a can be interpreted as the image of the O−Ba−O−Ba columns. This is supported by the simulated image shown at the inset.

The array of Ba atoms is revealed as constituted by two discontinuous lines of three and four bright dots. This zigzag arrangement can be understood as the succession of two consecutive c layers separated from a third one by two h layers, the whole set leading to a [4 dots−3 dots] blocks disposition. This contrast configuration is in agreement with a layer sequence (hhchhcc), that is, the second of the three polytypes described above. The ideal structural model corresponding to this sequence has been drawn in Figure 2b. It correctly represents the topological features of the structure.

From the nominal composition, not all octahedral interstices can be occupied. There exist two cation vacancies per unit cell in the B sublattice. The B cation deficiency must be accommodated as complete layers of vacant octahedral sites in such a way that the middle octahedron of each triplet remains empty since this ensures the largest separation between B cations.

The [1$\bar{1}$0] zone image is less informative, but it strikingly confirms the structure, as can be observed from comparison between the experimental image and the projected model of Figure 3b. According to the ideal structure, all atom columns are now aligned along the *c*-direction, and the cationic vacancy layers can be recognized. In thicker parts of the foil two lines of dark contrast perpendicular to the *c*-axis can be observed per unit cell, giving rise to blocks of three and four bright dots along *c*. This image interpretation agrees very well with the projected model, the dark lines corresponding to the cationic vacancy planes. The simulated image has been included for comparison.

As we have mentioned in the Experimental Section, the thermogravimetric analysis confirms the anionic composition to be O_{20}. This oxygen content would imply, in the most favorable case to be observed, one BaO_2 layer and six BaO_3 layers in the unit cell. A random distribution of the anionic deficiency in every Ba−O layer would also be possible and even a partial order inside only one type of layer (c or h). Since oxygen positions are usually not revealed in high-resolution images, it was not clear from the existing model whether the oxygen vacancies in $Ba_7Nb_4MoO_{20}$ were ordered or not.

Further structural analysis was then necessary, and the corresponding structural refinement by means of neutron diffraction data was performed. The proposed model described above was used as the starting point for the refinement. The formula corresponded to $Ba_7Nb_4MoO_{20}$ ($Z = 1$) and the atomic positions were Ba1 in *1a*, Ba2 and Ba3 in *2d*, with $z = 6/7$ and $z = 4/7$, respectively, Ba4 in *2c* ($z = 2/7$), M1 (M = Mo, Nb) in

(3) Rodríguez-Carvajal, J. *Physica B* **1993**, *192*, 55.
(4) Zhdanov, G. S. *Dokl. Akad. Nauk. SSSR.* **1945**, *48*, 40.
(5) Shannon, R. D.; Prewitt, C. T. *Acta Crystallogr.* **1969**, *B25*, 925.

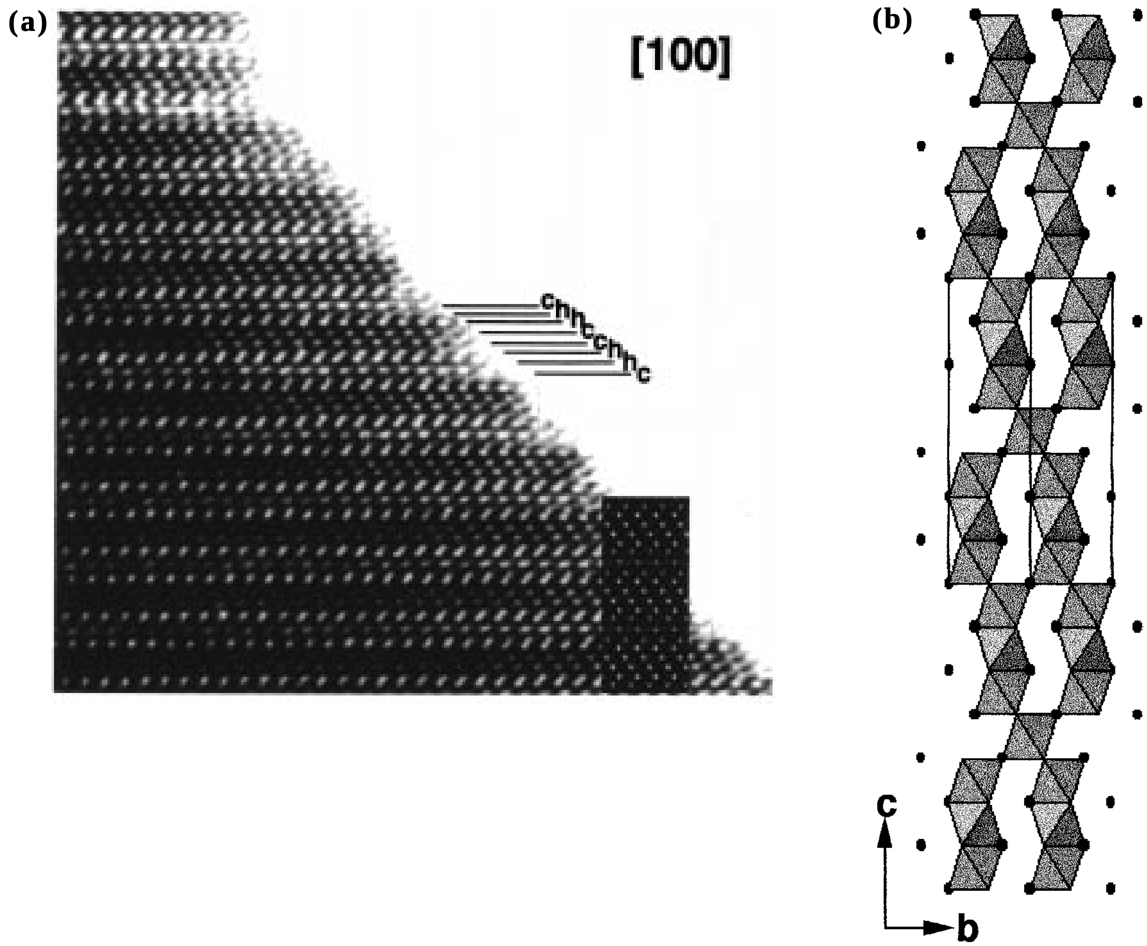

Figure 2. (a) HREM image of $Ba_7Nb_4MoO_{20}$ taken along the [100] zone axis. The calculated high-resolution image (thickness 5.0 nm and defocus −67 nm) in the same projection has been included for comparison, $C_s = 1$ mm, $\Theta = 0.55$ mrad. (b) Ideal structural model corresponding to the 7H sequence (hhchhcc).

1b, M2 and M3 in *2d* positions with $z = 1/14$ and $z = 5/14$, respectively, O1 in *3e*, and O2, O3, and O4 in *6i* [(1/6, 1/6, 1/7), (1/6, 1/6, 3/7), and (1/2, 0, 2/7)] in the $P\bar{3}m1$ space group (No. 164).

The main features of the crystal structure deal with the distribution of B cations and cation vacancies as well as with the anion vacancies location.

Mo and Nb atoms were distributed statistically in *1b* and *2d* positions, the cationic empty sites being located in *2d* with $z = 3/14$.

Different possibilities for the anionic vacancies accommodation were tested. Since the random distribution of the oxygen deficiency led to *R* values unacceptably high, we tried to accommodate it in only one type of layer, that is, in the h layers, provided that the central octahedra is empty, or in the c layers as it has been observed previously.[1] The attempt to place the anionic vacancies preferentially in the h layers improved somewhat the agreement between observed and calculated profile diagrams, but the *R* factors were still very high. The structural refinement when locating the oxygen deficiency in the c layers gave the best profile fit but the occupation factor of O1 in *3e* dropped drastically close to zero, indicating the absence of O1 from this site. It seemed then that the anionic vacancies were located mainly in this position, which would lead to BaO_2 composition in the corresponding layer and forseeable to tetrahedra formation. Hence, we propose that O1 is shifted to a *2d* position ($z = 0$) and therefore a tetrahedral coordination for Mo/Nb results.

Final structural refinement was carried out including this assumption, the profile fittings were good, and the structural data obtained were reasonable. Refinement details are summarized in Table 1. Atomic coordinates and isotropic thermal parameters are listed in Table 2. It is worth mentioning the unusually high value of the isotropic temperature factor of the O1 site, and we will go further on this fact.

Table 3 contains the important bond lengths and bond angles.

The observed, calculated, and difference neutron diffraction profiles are shown in Figure 4. Four small maxima in the profile were excluded in the refinement ($2\theta = 44.5$, 66.9, 107.5, and 113.5) which is accounted for by the presence of a very small amount of $BaMoO_4$.

Despite the existence of the two polyhedra types for the B cations, the different preference of Mo(VI) and Nb(V) to adopt octahedral or tetrahedral coordination was not considered, because of the similarity in the neutron scattering length and the X-ray scattering factor for the two cations as well as the small difference in ionic radii.[5]

The structure of $Ba_7Nb_4MoO_{20}$ is shown in Figure 5. It can be described as constituted by a [111] perovskite block of composition $Ba_4B_3O_{12}$ and a block (hch) of composition $Ba_3B_2O_8$. Going further in this description,

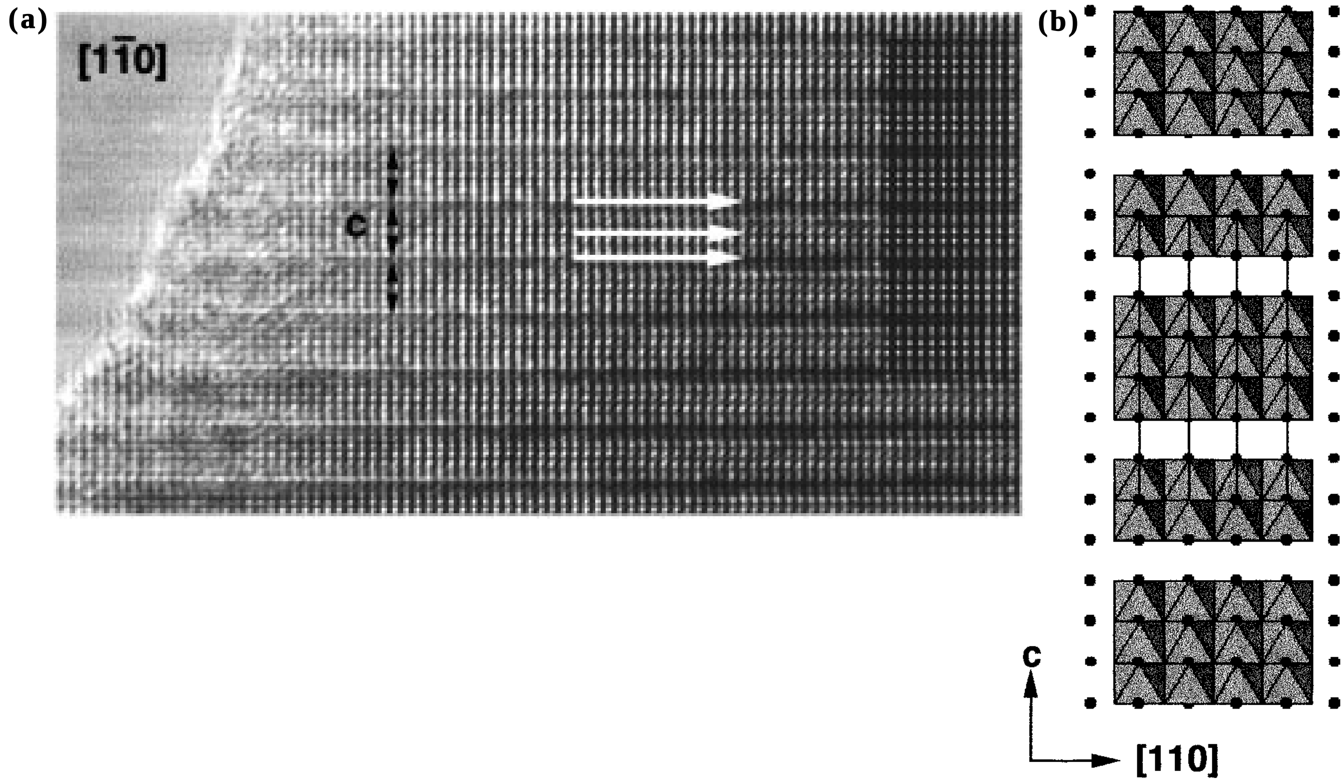

Figure 3. (a) HREM micrograph of $Ba_7Nb_4MoO_{20}$ in the [1$\bar{1}$0] projection. White arrows have been placed in the thicker part of the crystal to show the two dark contrast lines observed in the unit cell. The calculated high-resolution image (thickness 9.0 nm and defocus 70 nm) in the same projection has been included for comparison, C_s = 1 mm, Θ = 0.55 mrad. (b) Ideal structural model projected along the [1$\bar{1}$0] direction.

Table 1. Crystallographic and Experimental Data for $Ba_7Nb_4MoO_{20}$

space group	$P\bar{3}m1$
a (Å)	5.8644(2)
c (Å)	16.5272(4)
Z	1
V (Å^3)	492.251
radiation and wavelength	λ = 2.3433 Å (Ge-mono)
2θ range	3° ≤ 2θ ≤ 170°
R_F, R_B, R_{wP}	5.96, 6.01, 7.11
goodness of fit	7.89

Table 2. Atomic Parameters for $Ba_7Nb_4MoO_{20}$

atom	position	x/a	y/b	z/c	B_{iso} (Å^2)
Ba1	*1a*	0	0	0	0.8(1)
Ba2	*2d*	1/3	2/3	0.8236(6)	0.8(1)
Ba3	*2d*	1/3	2/3	0.5769(7)	0.8(1)
Ba4	*2c*	0	0	0.2812(6)	0.8(1)
(Nb,Mo)1	*1b*	0	0	0.5	1.3(1)
(Nb,Mo)2	*2d*	1/3	2/3	0.0943(5)	1.3(1)
(Nb,Mo)3	*2d*	1/3	2/3	0.3493(5)	1.3(1)
O1	*2d*	1/3	2/3	−0.0105(7)	6.1[a]
O2	*6i*	0.1738(7)	−0.1738(7)	0.1316(3)	1.38(7)
O3	*6i*	0.1638(8)	−0.1638(8)	0.4323(3)	1.38(7)
O4	*6i*	0.5	0	0.2939(3)	1.38(7)

[a] See text.

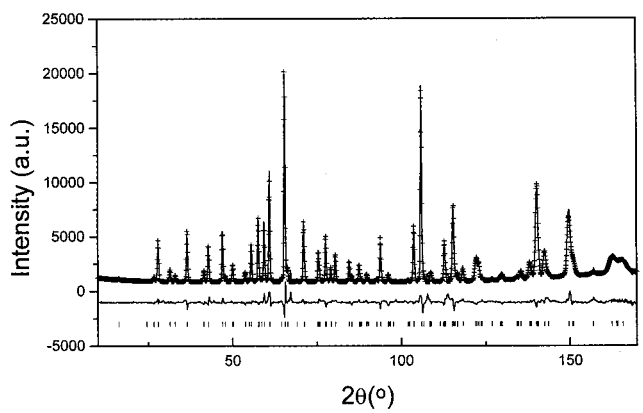

Figure 4. Observed, calculated, and difference powder neutron diffraction patterns of $Ba_7Nb_4MoO_{20}$.

Table 3. Main Interatomic Distances (Å) for $Ba_7Nb_4MoO_{20}$

Ba1−O1	3.39(1)	×6	M1−O3	2.00(1)	×6
Ba1−O2	2.80(2)	×6	M2−O1	1.74(9)	×1
Ba2−O1	2.74(6)	×1	M2−O2	1.71(3)	×3
Ba2−O2	3.02(4)	×6	M3−O3	2.20(2)	×3
Ba2−O4	2.58(2)	×3	M3−O4	1.91(6)	×3
Ba3−O3	2.93(4)	×9			
Ba3−O4	2.72(1)	×3			
Ba4−O2	3.04(6)	×3			
Ba4−O3	3.00(2)	×3			
Ba4−O4	2.94(2)	×6			

the first block has a (hcch) sequence which is in fact one-third of the 12R $A_4B_3O_{12}$ (hcch)$_3$ and the second one is one-third of the palmierite unit cell 9R (hch)$_3$ of composition $A_3B_2O_8$. Therefore, the unit cell of $Ba_7Nb_4MoO_{20}$ can be seen as an ordered intergrowth of the structural units corresponding to the 12R and the palmierite polytypes. Both types of blocks are isolated through the cationic vacancies and are stacked in a hexagonal disposition, one with respect to the other. Thus, the structure is quasi-bidimensional.

As we have previously mentioned, the corresponding unshared tetrahedral corner oxygen O1 has a quite high isotropic temperature factor. It suggests a high mobility of the oxygen atom in this position and this fact does not reflect the thermal stability of the phase toward oxygen composition that we have found experimentally. Therefore, it must be associated to local disorder of the anionic vacancies inside the BaO_2 cubic layer. This

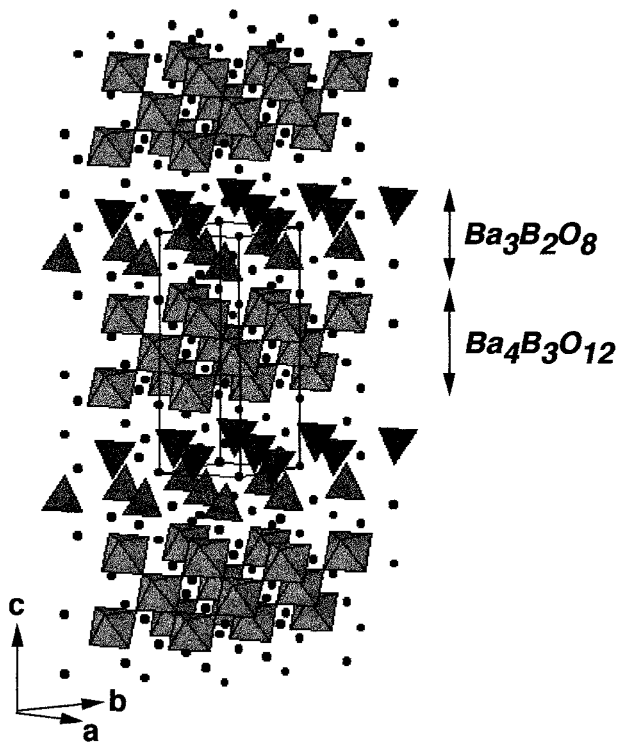

Figure 5. Crystal structure of $Ba_7Nb_4MoO_{20}$ showing the ordered intergrowth between the $Ba_4B_3O_{12}$ and $Ba_3B_2O_8$ blocks that constitute the unit cell.

disordered distribution would lead to five- and/or six-coordination sites, and to the corresponding change in the local composition, probably compensated by the presence of oxygen substoichiometry in any of the BaO_3 layers. All these factors would have little significance in introducing serious changes in the structure proposed.

Such high B_{iso} values in equivalent oxygen sites have been previously obtained in the structural refinement of the $BaVO_{3-y}$ phases.[6] The authors attribute the mobility of the unshared oxygen atom to the instability of the system toward oxidation−reduction, and therefore to the change in both coordination number and formal charge of the vanadium atoms. As can be seen in Table 3, there are two types of nonequivalent positions of the B cations in octahedral coordination: in the center of the (hcch) block (Nb, Mo)1 and adjacent to the B-empty site (Nb, Mo)3. (Nb, Mo)1 is placed on a regular octahedron and the distance (Nb, Mo)1−O3 = 2.00(1) Å is very close to the bond length expected using the ionic radii compiled by Shannon:[5] 1.99 Å for NbO_6^{7-} and 1.94 Å for MoO_6^{6-}. The cation vacancy location leads to a shift of the (Nb, Mo)3 cations along the *c*-axis away from the centers of the octahedra toward the triangular face formed by the O4 atoms which are shifted, resulting in a (Nb, Mo)3−O4 distance of 1.91(6) Å and a (Nb, Mo)3−O3 bond length of 2.20(2) Å. As a consequence, the (Nb, Mo)3 atoms have a distorted coordination.

The (Nb, Mo)2 atoms are placed on quasi-regular tetrahedral polyhedra as can be observed when comparing the (Nb, Mo)2−O1 and (Nb, Mo)2−O2 bond lengths.

The expected Mo(VI)−O and Nb(V)−O distances[5] are 1.76 and 1.83 Å, respectively, in a tetrahedral environment. The average observed (Nb, Mo)−O bond length for the (Nb,Mo)2 tetrahedra (1.73 Å) would suggest the preferential occupation of the *1b* site of the structure by molybdenum atoms. However, short distances Nb−O (1.66 Å) have been previously found for NbO_4^{3-} tetrahedra in Nb_2O_5[7] and, therefore, the structural refinement does not allow one to ellucidate the presence of cationic order in the B sublattice.

Vibrational spectroscopy can provide information of value when interpreted in conjunction with the known structural features and, in this sense, the Raman spectroscopy study of $Ba_7Nb_4MoO_{20}$ and related Ba−Mo/Nb−O phases is in progress and will be reported in due course.

To our knowledge, this is the first time that a 7H polytype is stabilized for cation-deficient perovskite oxides. In all the systems described in the literature,[8−11] the most extensively studied A:B ratio corresponds to A:B::n:(n−1) and the stacking sequences adopted can be formulated as (n−2)c h h, that is, blocks of (n−2) cubic layers separated by a plane of cation vacancies. Thus, n = 3 has the sequence 9R $(chh)_3$, the n = 4 belongs to the 12R polytype [$(hcch)_3$], n = 5 is 5H with a (hccch) sequence, and n = 6 adopts 18R type [$(hccccch)_3$]. Following this description, the $(hcccccch)_3$ sequence should correspond to n = 7, with a 21R polytype. In a recent study, Pasero et al.[12] have found a well-ordered example of the n = 7 compound in the $Sr_n(Nb,Ti)_{n-1}O_{3n}$ system. Although the authors have studied this phase by electron microscopy, they neither provide information about the symmetry and the metric of the unit cell nor analyze the layer stacking sequence. However, when carefully observing the HREM image of Figure 8 on ref 12 and after doing the Fourier transform of this micrograph, it is easy to obtain the unit cell of the phase with rombohedral symmetry and hexagonal lattice parameters $a \approx 5.7$ Å and $c \approx 40$ Å, corresponding to the 21R polytype with stacking sequence $(hcccccch)_3$ as predicted above for a $n = 7$, $\delta = 1$ compound.

The hh pair present in all the above structural blocks can only stabilize one cation vacancy per formula. The existence of two empty B positions in the present case is probably the reason for the unusual 7H polytype being adopted.

Acknowledgment. We acknowledge Dr. J. Rodriguez-Carvajal at the Laboratoire Leon Brillouin for collecting the powder neutron diffraction data. We would like to thank Dr. U. Amador for valuable discussions in interpreting the neutron diffraction data. We are also grateful to the Centro de Microscopía Electrónica (UCM) for facilities, and specially to J. L. Baldonedo and P. Robredo for technical assistence as well as valuable help in figures production. We acknowledge the financial support of CICYT (Spain) through Research Project MAT95-0642.

CM981011I

(6) Liu, G.; Greedan, J. E. *J. Solid State Chem.* **1994**, *110*, 274.

(7) McConell, A. A.; Anderson, J. S.; Rao, C. N. R. *Spectrochim. Acta* **1976**, *32A*, 1067.

(8) Bontchev, R.; Weill, F.; Darriet, J. *Mater. Res. Bull.* **1992**, *27*, 931.

(9) Van Tendeloo, G.; Amelinckx, S.; Darriet, B.; Bontchev, R.; Darriet, J.; Weill, F. *J. Solid State Chem.* **1994**, *108*, 314.

(10) Shpanchenko, R. V.; Nistor, L.; Van Tendeloo, G.; Van Landuyt, J.; Amelinckx, S.; Abakumov, A. M.; Antipov, E. V.; KovBa, L. M. *J. Solid State Chem.* **1995**, *114*, 560.

(11) Abakumov, A. M.; Van Tendeloo, G.; Scheglov, A. A.; Shpanchenko, R. V.; Antipov, E. V. *J. Solid State Chem.* **1996**, *125*, 102.

(12) Pasero, D.; Tilley, R. J. D. *J. Solid State Chem.* **1998**, *135*, 260.